ACS APPLIED MATERIALS & INTERFACES

www.acsami.org

Research Article

Stretching-Tunable High-Frequency Magnetic Properties of Wrinkled CoFeB Films Grown on PDMS

Jian Liu, Jinan Chen, Yanran Zhang, Shangjie Fu, Guozhi Chai,* Cuimei Cao, Xiaoyan Zhu, Yongbin Guo, Wenjuan Cheng, Dongmei Jiang, Zhenjie Zhao, and Qingfeng Zhan*

Cite This: *ACS Appl. Mater. Interfaces* 2021, 13, 29975−29983

Read Online

ACCESS | Metrics & More | Article Recommendations

ABSTRACT: We demonstrated a convenient method via applying uniaxial tensile strains to continuously tune the high-frequency properties of flexible magnetic films. CoFeB films were magnetron sputtered onto prestretched polydimethylsiloxane (PDMS) membranes. They exhibit a self-assembled periodic wrinkling surface structure because of the large mismatch of Young's moduli between the elastomeric PDMS substrates and the metal layers. The wrinkling morphology and the residual tensile stress caused by the Poisson effect can be continuously tuned by a uniaxial stretching strain less than the growth prestrain, which consequently results in changes in high-frequency performance. The initial permeability and the ferromagnetic resonance frequency of flexible CoFeB thin films can be monotonously tuned in wide ranges of about hundreds and 1 GHz, respectively. A good repeatability over thousands of stretching-relaxing cycles has been demonstrated without any obvious reduced high-frequency properties. This flexible CoFeB films with excellent stretching-tunable high-frequency performances are promising for application in flexible and tunable microwave devices.

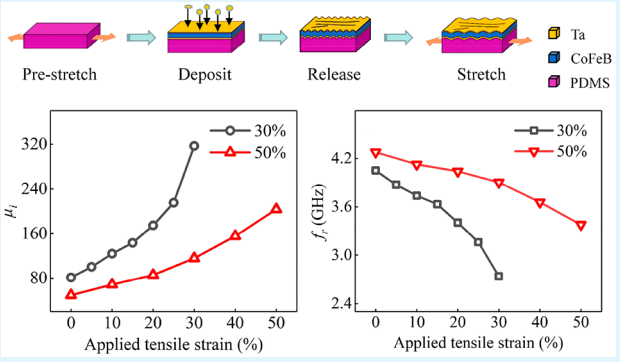

KEYWORDS: *stretching tunable, high frequency, flexible magnetic films, wrinkling topography, CoFeB*

INTRODUCTION

Soft magnetic thin films, which can be used in high-frequency devices such as filters, planar inductors, and tunable resonator, have excited great research interest because of the rapid development of microwave technologies and the increasing demand for miniaturization in microwave devices.[1−3] In the previous investigations, most magnetic films applied in microwave devices were fabricated on conventional rigid substrates such as silicon and glass.[4−6] Recently, with the popularity of flexible electronics, high-frequency devices have been fabricated on flexible substrates for potential applications in wearable wireless transmission systems and reconfigurable electromagnetic interference shielding.[7,8] Compared with conventional rigid devices, flexible high-frequency devices have the advantages of lightweight, enhanced durability, mechanical flexibility, and mountability on uneven surfaces.[9−13] In addition, flexible high-frequency devices often exhibit an excellent tunability by mechanical strains.[14−17] Liu et al. fabricated split ring resonators for electromagnetic interference shielding metamaterials by attaching silver nanowires onto prestrained polydimethylsiloxane (PDMS).[8] The geometry and electromagnetic properties of the resonators would change when subjected to a mechanical strain, so that the operating frequency could be continuously tuned in the X-band through the mechanical strain.

The complex permeability ($\mu = \mu' - i\mu''$) and ferromagnetic resonance (FMR) frequency f_r are two important factors of soft magnetic thin films. They determine whether soft magnetic thin films are suitable for the specific application in high-frequency devices. For instance, soft magnetic films used in planar inductors are required to possess relatively high μ' and low μ'', and a high f_r is also needed to exceed the operating frequency of the devices.[18] Therefore, numerous research efforts, such as oblique deposition, annealing in magnetic field, and exchange bias, have been made to change the complex permeability and the FMR frequency of magnetic films to meet various requirements of applications.[19−21] For example, Li et al. demonstrated that when the angle of oblique deposition increases from 10 to 70°, the ferromagnetic resonance frequency can be enhanced from 2.83 to 9.71 GHz and the

Received: April 21, 2021
Accepted: June 7, 2021
Published: June 18, 2021

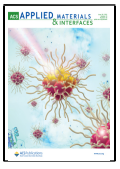

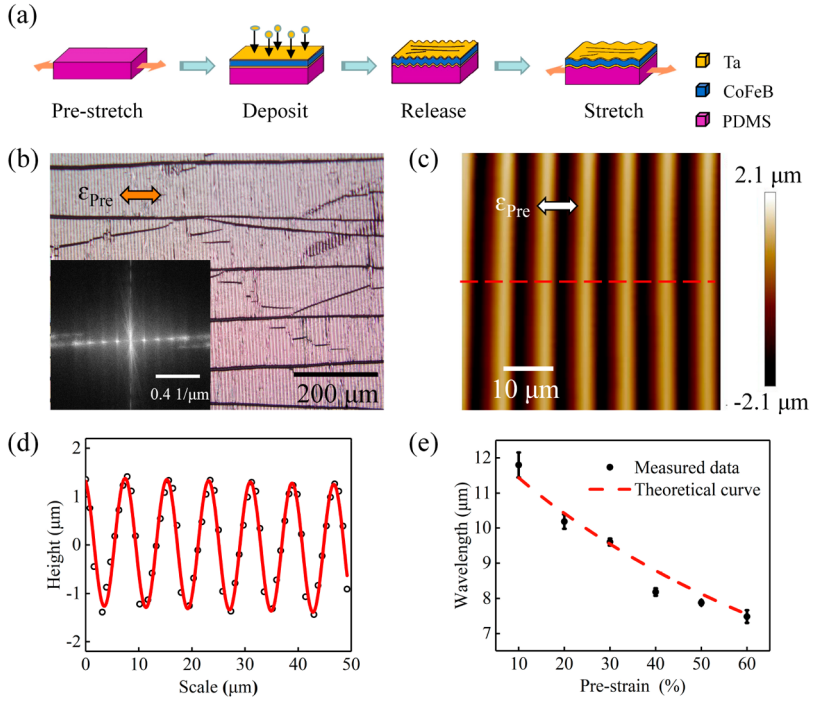

Figure 1. (a) Illustrative drawings for wrinkled CoFeB films grown on prestrained PDMS membranes. (b) Optical image of the wrinkled CoFeB film fabricated with 50% prestrain and the corresponding FFT image. (c) Surface topography of the sample fabricated with 50% prestrain measured by AFM and (d) cross-sectional view extracted along the red dashed line (black circles, measured data; red line, sinusoidal fitting). (e) Wrinkle wavelength as a function of the prestrain applied during fabrication. The dashed line is the result of theoretical fitting based on the elastic model.

initial permeability is reduced from 370.6 to 31.4.[22] This method can only statically tune the high-frequency properties of magnetic films. Recently, magnetic properties to be controlled by mechanical stress, magnetoelectric coupling, and magnetoelastic coupling have aroused wide research interests because of the advantages of convenience and low energy consumption.[23] The electric field applied on a multiferroic heterostructure can dynamically tune the high-frequency properties. Lou et al. prepared multiferroic FeGaB/PZN−PT heterostructures that exhibit a large tunable FMR frequency ranging from 1.75 to 7.57 GHz by applying an electric field.[24] For the electric control of high-frequency properties, ferroelectric layers or substrates are often required, which makes them hard to integrate in standard microelectronics processes. A flexible substrate is easy to load with mechanical stress, which brings great convenience to tune the magnetic properties. Years ago, Dai et al. showed that the magnetic anisotropy of flexible magnetostrictive FeGa films fabricated on polyethylene terephthalate (PET) can be continuously changed by applying a bending strain.[25] The excellent strain-tunable magnetic anisotropy inspirits that the high-frequency properties of flexible magnetic films could be tuned by strains. Yu et al. demonstrated that a bending strain of PET substrates preset in the fabricate process can tune the FMR frequency of FeGa films.[26] Most recently, Li et al. fabricated flexible FeCoTa films grown on PDMS with a wrinkling surface, and the high-frequency properties could be tuned by altering the applied prestrain during growth.[27] However, so far, the continuous control of high-frequency properties has not yet been reported in flexible soft magnetic films. Previous studies have shown that such films with wrinkling surface morphologies are stretchable.[28] When applying a tensile strain to the films, the wrinkling surface structure will be flattened according to an elastic model,[29] resulting in changes in magnetic performance. Taking advantage of this trait, high-frequency properties of magnetic films with wrinkling surface morphologies are expected to be continuously tuned by mechanical strains. The way to change high-frequency properties of magnetic films will be greatly simplified and the application of magnetic films in flexible high-frequency devices can be broadened to many novel electromagnetic devices, such as phase shifters, tunable resonators, and tunable filters.

In this study, we employed a self-assembled wrinkling surface structure on PDMS to fabricate flexible soft magnetic films by a method of prestretching the elastomeric substrates. $Co_{40}Fe_{40}B_{20}$ (CoFeB) alloy was chosen as the ferromagnetic layer because it has been widely utilized for cores in high-frequency inductors and microwave integrated circuits.[30] The flexible CoFeB films grown on PDMS show a uniaxial magnetic anisotropy parallel to the surface wrinkles and displays good high-frequency performances with initial permeability μ_i varied between 35 to 154 and f_r changed between 3.4 to 4.4 GHz by changing the prestrain. When a uniaxial tensile strain is applied to the CoFeB films, the wrinkling surface morphology is flattened as predicted by theory, the transverse residual tensile stress in the films is gradually relaxed. Thus, μ_i can be continuously varied in a range of hundreds and f_r can be changed in a range of 1 GHz. The continuous tunability of the high-frequency performances of magnetic films may open a new way to develop mechanical strain tunable high-frequency devices, especially in wide-frequency-range applications.

RESULTS AND DISCUSSION

Figure 1a schematically exhibits the processes to fabricate stretchable CoFeB films with a wrinkling morphology. PDMS

https://doi.org/10.1021/acsami.1c07384
ACS Appl. Mater. Interfaces 2021, 13, 29975−29983

membranes with 350 μm in thickness are uniaxially prestretched with different prestrains ε_{pre} by a homemade stretching apparatus. A Ta buffer layer with 10 nm thickness is first deposited on the prestretched PDMS substrates to prevent the ferromagnetic atoms from being sputtered into the PDMS membranes. Then, a ferromagnetic CoFeB layer with 50 nm in thickness and a Ta capping layer with 5 nm in thickness are deposited in sequence. After releasing the prestrain, a wrinkling morphology is formed on the sample surface because of the large mismatch of Young's moduli between the compliant PDMS substrates and the rigid metal layers.[31] Because of the Poisson effect, the elastomeric PDMS substrates display an elongation $\varepsilon_L = \nu_s\varepsilon_{pre}$ perpendicular to the prestretching direction. The Poisson's ratio of PDMS ν_s is determined as 0.42 by measuring the transverse shrinkage during a longitudinal stretching. The transverse tensile strain caused by the Poisson effect is by far larger than the stretching limit of metals (less than 1%), which leads to cracks of metal layers along the prestretching direction. Figure 1b shows a typical optical image of the wrinkled CoFeB sample fabricated with ε_{pre} = 50%. The periodic change in contrast indicates the formation of wrinkling morphology over a large area of several cm^2. There are several cracks along the prestretching direction with an average crack width of 8.3 μm and an average width of 72.2 μm for the cracked film, i.e., the intercrack distance. In addition, there are some small bifurcating cracks not completely along the prestretching direction. As a large growth prestrain is hard to uniformly apply and release in experiments, the bifurcating cracks obviously increase with increasing the prestrain. The formation of cracks can only partially release the lateral tensile stress that is caused by the Poisson effect during relaxing the growth prestrain. Li et al. demonstrated that an aggravated tensile stress remains to be concentrated at the boundaries of artificial cracks for wrinkled metallic multilayers mounted on PDMS.[32] The strength of the residual tensile stress for a wrinkled film in the releasing state is dependent on the growth prestrain. The periodicity of the wrinkling morphology in the real space can be transferred to a group of bright spots in the frequency space by fast Fourier transforms (FFT) of the optical image, as shown in the inset of Figure 1b. The distance from the first-order spot to the image center is inversely proportional to the wrinkle wavelength. Thus, the wavelength can be obtained as 7.9 μm by measuring the distance from the spot to the center of the image. Figure 1c shows the corresponding atomic force microscope (AFM) image in 50 × 50 μm^2. The wrinkles are nicely parallel to each other, showing an excellent periodicity. The cross-sectional view of the wavelike pattern can be nicely fitted to a sinusoidal curve with a wavelength of 7.8 μm and an amplitude of 1.3 μm, as shown in Figure 1d. The wavelength is consistent with the value obtained from the FFT image. Figure 1e shows the wavelength obtained by FFT of the optical images for the wrinkled CoFeB films. With increasing the growth prestrain from 10 to 60%, the wavelength decreases from 11.8 to 7.4 μm. The morphology can be theoretically predicted by an elastic model with minimizing the total strain energy consisting of the stretching strain energy and the bending strain energy in wrinkled films. The wavelength can be theoretically obtained as[28]

$$\lambda = \frac{1+\varepsilon_{app}}{(1+\varepsilon_{pre})(1+\varepsilon_{app}+\zeta)^{1/3}}\cdot\frac{\pi t_f}{\sqrt{\varepsilon_c}} \quad (1)$$

where $\varepsilon_c = 0.52\left[\frac{E_s(1-\nu_f^2)}{E_f(1-\nu_s^2)}\right]^{2/3}$ is a threshold strain for buckling and producing a wrinkling morphology, $\zeta = \frac{5}{32}(\varepsilon_{pre}-\varepsilon_{app})(1+\varepsilon_{pre})$, ε_{app} = 0 is the applied tensile strain for films in the fully releasing state, t_f = 65 nm is the total thickness of metal films, E_s = 3.4 MPa and E_f = 300 GPa are the Young's moduli for PDMS and metal films, respectively, and ν_f = 0.3 is the Poisson's ratio for metal films. As shown in Figure 1e, the theoretical morphological wavelengths for the wrinkled CoFeB films can be calculated by using these parameters, which agree well with the experimental values.

The mechanical stretchability of the wrinkled CoFeB films is characterized by applying a uniaxial tensile strain along the prestretching direction. Figure 2a shows the optical images of the wrinkling morphology when a uniaxial tensile strain is applied on the wrinkled CoFeB film fabricated with ε_{pre} = 30%. The contrast between the peak and trench of the wrinkles is clearly reduced with increasing the tensile stain, indicating that the wrinkling morphology is gradually flattened by uniaxial tensile stretching the films. As revealed on the right side of the images, the corresponding first order FFT spots gradually approach to the image center with increasing the tensile strain, indicating the increase in the wavelength of wrinkling

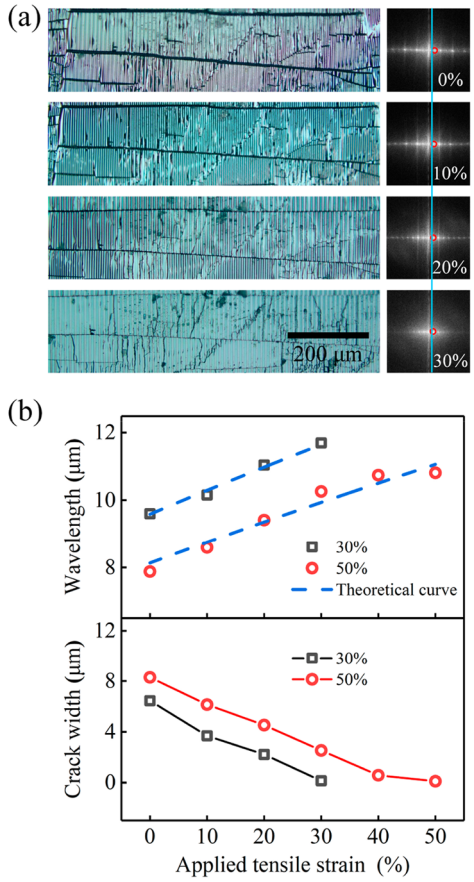

Figure 2. (a) Optical images of the CoFeB film fabricated with 30% prestrain when applying different uniaxial tensile strains. The corresponding FFT images are presented on the right side. (b) Surface morphologic wavelength and crack width as a function of the applied tensile stain for the samples fabricated with 30 and 50% prestrains. The dashed lines are the theoretical fittings.

https://doi.org/10.1021/acsami.1c07384
ACS Appl. Mater. Interfaces 2021, 13, 29975−29983

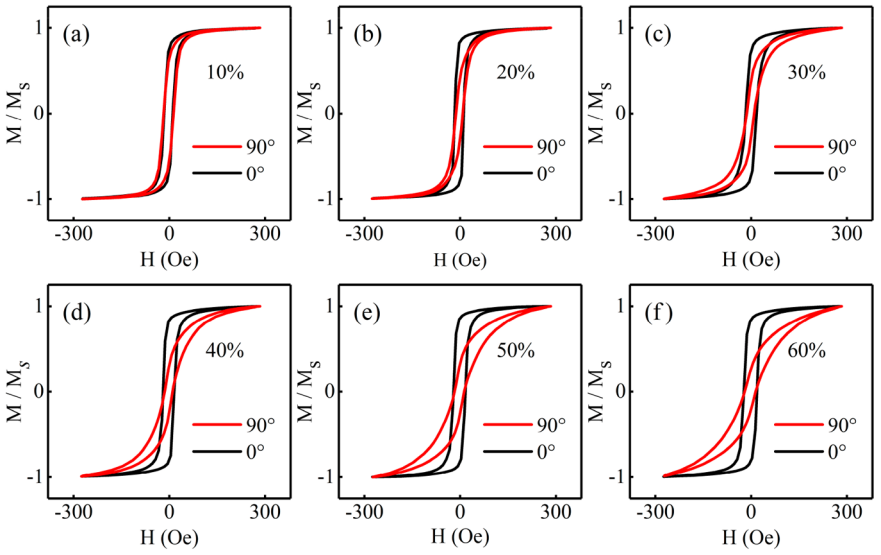

Figure 3. Hysteresis loops for wrinkled CoFeB films fabricated with different prestrains of (a) 10, (b) 20, (c) 30, (d) 40%, (e) 50, and (f) 60%. The magnetic field during tests is applied in-plane parallel (θ = 0°) and perpendicular (θ = 90°) to the wrinkles.

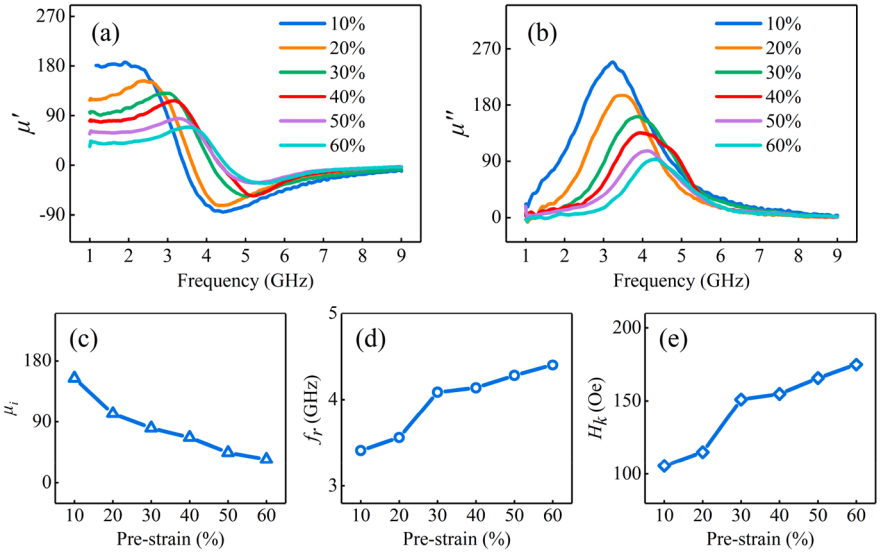

Figure 4. (a) Real and (b) imaginary permeability spectra measured at zero magnetic field for wrinkled CoFeB films fabricated with growth prestrains ranging from 10 to 60%. (c) Initial permeability and (d) ferromagnetic resonance frequency as a function of the growth prestain. The data are extracted by fitting the permeability spectra to the LLG equation. (e) Magnetic anisotropy field as a function of the growth prestrain. The data are obtained by substituting the ferromagnetic resonance frequency into the Kittel equation.

morphology. For the film fabricated with ε_{pre} = 30%, the wavelength increases from 9.6 to 11.7 μm as the tensile strain increases from 0 to 30%. For the film grown with ε_{pre} = 50%, the wavelength increases from 7.8 to 10.8 μm as the tensile strain increases from 0 to 50%, as shown in Figure 2b. The applied tensile strain dependence of wavelength can also be theoretically explained by the elastic model of eq 1. As shown in Figure 2b, the theoretical wavelengths agree well with the experimental results when the CoFeB films are in the elastic deformation region that is less than the growth prestrain. The films start to break perpendicular to the stretching direction when the applied tensile strain is larger than the growth prestrain. Therefore, the mechanical stretchability of the wrinkled CoFeB films roughly equals to the growth prestrain and hence can be preset by changing the prestrain during the sample fabrication. It should be noted that the applied tensile strain can only be loaded along the direction of the growth prestrain, because the one-dimensional wrinkling surface structure is formed perpendicular the growth prestrain. A tensile strain applied perpendicular to the prestrain may crash the wrinkled CoFeB film. The average width of the film cracks along the prestretching direction significantly decreases with the tensile strain applied along the prestrain direction due to the Poisson effect. For the film fabricated with ε_{pre} = 30%, the crack width decreases from 6.4 μm to 0 as the applied tensile strain increases from 0 to 30%. For the sample of ε_{pre} = 50%, the crack width decreases from 8.3 μm to 0 with increasing the applied tensile strain from 0 to 50%, as shown in Figure 2b. The average width of cracked films, i.e., the intercrack distance, does not obviously change in both the releasing and stretching processes, indicating the area covered by the metal films is subjected to a residual tensile stress along the lateral direction

https://doi.org/10.1021/acsami.1c07384
ACS Appl. Mater. Interfaces 2021, 13, 29975−29983

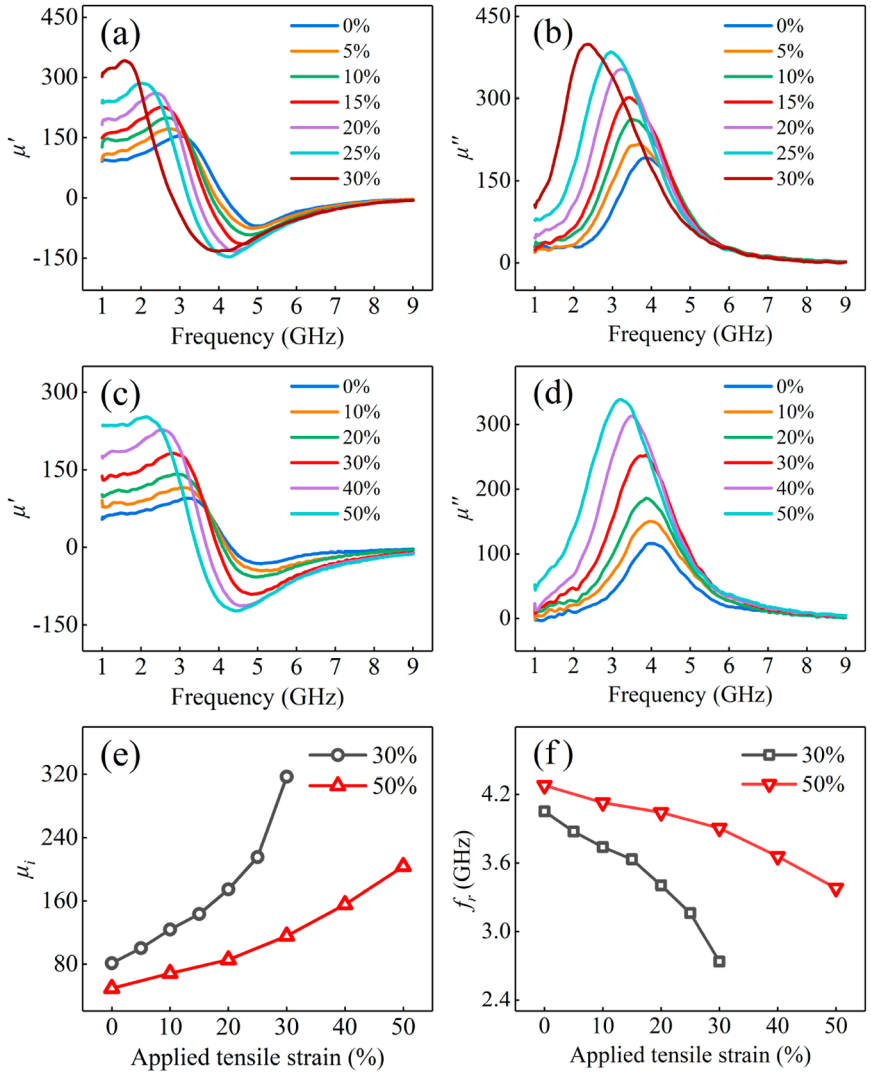

Figure 5. (a) Real and (b) imaginary permeability spectra measured by applying different tensile strains for the wrinkled CoFeB film fabricated with 30% prestrain. (c) Real and (d) imaginary permeability spectra measured by applying different tensile strains for the wrinkled CoFeB film fabricated with 50% prestrain. The applied tensile strain is less than the growth prestrain. The applied tensile strain dependence of (e) initial permeability and (f) ferromagnetic resonance frequency for the wrinkled CoFeB films fabricated with 30 and 50% prestrains.

caused by the Poisson effect. The lateral expansion and contraction of the wrinkled samples caused the Poisson effect are reflected in the increase and decrease of the crack width. The decrease in the average width of the film cracks in the stretching process indicates that the residual tensile stress in the CoFeB films along the lateral direction is gradually relaxed by applying a longitudinal tensile strain.

Figure 3 shows the magnetic hysteresis loops measured with an in-plane magnetic field parallel (θ = 0°) and perpendicular (θ = 90°) to the wrinkles of CoFeB films. All the films fabricated with different prestrains exhibit a relatively square loop at θ = 0° and a slanted one at θ = 90°, indicating an in-plane uniaxial magnetic anisotropy along the wrinkles. The uniaxial magnetic anisotropy originates from the combined effects of the residual tensile stress and the wrinkling surface morphology. On one hand, the residual tensile stress lateral to the growth prestrain may produce a uniaxial magnetic anisotropy along the wrinkles because of the positive magnetostriction about 30 ppm of CoFeB.[33] On the other hand, magnetic charges may be created on the wrinkling morphology when an in-plane magnetic field is applied perpendicular to the wrinkles. The dipolar interaction between the magnetic charges can produce an equivalent field to parallel align the magnetic moments along the wrinkles, i.e., a uniaxial magnetic anisotropy.[34] In addition, magnetic charges may also be created on the edges of cracks when applying an in-plane magnetic field, which may give rise to an additional magnetic anisotropy along the cracks. As the crack width is in the magnitude of 8 μm, the induced magnetic anisotropy field is estimated to be less than 2 Oe.[35] In comparison with the magnetic anisotropy caused by the residual tensile stress and the wrinkling morphology, the magnetic anisotropy induced by the cracks is very weak and plays a less important role on the high-frequency properties. With increasing the growth prestrain from 10 to 60%, the remanence ratio M_r/M_s of hysteresis loops measured along the surface wrinkles increases from 0.67 to 0.83, indicating the increase in uniaxial magnetic anisotropy. The coercivity correspondingly increases from 14 to 21 Oe. For the measurements perpendicular to the surface wrinkles, the value of M_r/M_s obviously decreases from 0.60 to

https://doi.org/10.1021/acsami.1c07384
ACS Appl. Mater. Interfaces 2021, 13, 29975−29983

0.18 with increasing the prestain from 10 to 60%, but the coercivity keeps around 15 Oe.

The high-frequency magnetic properties of the wrinkled CoFeB films were measured by using a vector network analyzer with the shorted microstrip transmission-line perturbation method.[18] Figure 4a, b shows the dynamic real μ' and imaginary μ'' parts of complex permeability spectra of wrinkled CoFeB films measured at a zero magnetic field and in a frequency f ranging from 1 to 9 GHz. With the increase in frequency, μ' shows a dispersive shape curve, whereas μ'' shows a Lorentzian type resonance curve, indicating a resonance type permeability spectrum. The initial permeability μ_i of the wrinkled CoFeB films decreases with increasing the prestrain, while the ferromagnetic resonance (FMR) frequency f_r corresponding to the resonance peak of μ'' shifts toward a higher value. The complex permeability spectra can be quantitatively described by solving the Landau−Lifshitz−Gilbert (LLG) equation as[36]

$$\mu' = 1 + \chi_i \frac{1 - (1+\alpha^2)\left(\frac{f}{f_r}\right)^2}{\left[1 - (1+\alpha^2)\left(\frac{f}{f_r}\right)^2\right]^2 + \left[2\alpha\left(\frac{f}{f_r}\right)^2\right]^2} \quad (2)$$

$$\mu'' = \chi_i \frac{\left[(2\alpha)\left(\frac{f}{f_r}\right)\right]^2}{\left[1 - (1+\alpha^2)\left(\frac{f}{f_r}\right)^2\right]^2 + \left[2\alpha\left(\frac{f}{f_r}\right)^2\right]^2} \quad (3)$$

where $\chi_i = \mu_i - 1$ is the initial susceptibility and α is the damping constant. By means of fitting the complex permeability spectra to eqs 2 and 3, the damping constant α is obtained as 0.055, which is obviously higher than the intrinsic damping value of 0.002 for the counterpart grown on Si. The large value of α indicates a nonintrinsic damping, which is usually interpreted by the local resonance model and the two-magnon model occurring in an inhomogeneous film.[37] With increasing the growth prestrain from 10 to 60%, μ_i decreases from 311 to 35, and f_r increases from 2.3 to 4.4 GHz, as respectively illustrated in Figure 4c, d. The opposite prestrain dependence μ_i and f_r can be interpreted by using the Acher's limit of thin film:[38] $(\mu_i - 1)f_r^2 = [(\gamma/2\pi)4\pi M_s]^2$. For magnetic films with a certain saturation magnetization M_s, the increase in f_r may result in a decrease in μ_i. Therefore, to obtain both high values of both μ_i and f_r in magnetic thin films, magnetic materials with a high M_s such as CoFeB are necessary to be chosen. The magnetic anisotropy field H_k of the wrinkled CoFeB films can be obtained by using the Kittel equation:[39] $f_r = \frac{\gamma}{2\pi}\sqrt{(4\pi M_s + H_k)H_k}$, where the gyromagnetic ratio γ is 17.6 MHz/Oe and M_s of CoFeB films is experimentally obtained as 1110 G. H_k increases from 106 to 174 Oe as the prestrain increases from 10 to 60%, as shown in Figure 4e. According to the relation $\Delta f = \gamma\alpha(4\pi M_s + 2H_k)/2\pi$, the frequency line width Δf is shown to slightly increase from 1.98 to 2 GHz with the growth prestrain increasing from 10 to 60%. In comparison with the films prepared on Si, the frequency line width of the wrinkled CoFeB films are relatively large, which is presumably ascribed to the distribution of uniaxial magnetic anisotropy caused by the wrinkling morphology and the residual tensile stress. The relatively large line width can be reduced by using a relatively small prestrain to produce flexible magnetic films with a relatively low wrinkling amplitude, but which may sacrifice the stretchability of wrinkled films.

To investigate the high-frequency characteristics in a tensile stretching process, the permeability spectra of the wrinkling CoFeB films grown with ε_{pre} = 30% and 50% were measured under different tensile strains applied along the prestrain direction, as shown in Figure 5a−d. The measured permeability spectra change remarkably with the applied tensile strain, indicating the high-frequency performances of the wrinkled CoFeB films are sensitive to the stretching operation. Figure 5e, f, respectively, display the applied tensile strain dependence of μ_i and f_r obtained by fitting the permeability spectra to eqs 2 and 3. For the film grown with ε_{pre} = 30%, the value of μ_i monotonously increases from 81 to 317 and f_r decreases from 4.05 to 2.74 GHz as the applied tensile strain increases from 0 to 30%. For the film grown with ε_{pre} = 50%, μ_i increases from 49 to 204 and f_r decreases from 4.28 to 3.38 GHz as the applied tensile strain increases from 0 to 50%. Our experimental results indicate the high-frequency performances can be continuously tuned by applying a tensile strain less than the growth prestrain, which makes the wrinkled CoFeB films attractive for the application in tunable microwave devices. The tunability of high-frequency properties of the wrinkled CoFeB films can be qualitatively interpreted by considering the changes of both the wrinkling morphology and the residual tensile stress in the tensile stretching process. The applied tensile strain may gradually flatten the wrinkling morphology. Thus, the uniaxial magnetic anisotropy resulting from the distribution of magnetic charges on the wrinkling morphology correspondingly decreases with increasing the stretching strain. In addition, the residual tensile stress, which is caused by the Poisson effect when releasing the growth strain and exists in the area covered by the metal films, can be gradually relaxed in the stretching process. Consequently, the uniaxial magnetic anisotropy caused by the residual tensile stress through the positive magnetostriction of CoFeB may also decreases with stretching the wrinkled films. Therefore, the decrease of uniaxial magnetic anisotropy leads to the decrease in f_r according to the Kittel equation and the increase in μ_i due to the Acher's limit.

To assess the repeatability for the strain tuning of high-frequency properties in the wrinkled CoFeB films, the fatigue test was conducted by loading 2000 cycles of stretching and releasing strains on the wrinkled CoFeB films fabricated with ε_{pre} = 30 and 50%. In each cycle, uniaxial tensile strains were applied along the prestrain direction in a sequence of 0 → 25% → 15% → 0 for the film with ε_{pre} = 30% or in a sequence of 0 → 45% → 35% → 25% → 0 for the film with ε_{pre} = 50%. The permeability spectra were recorded after hundreds of stretching cycles. Figure 6a, b, respectively, show the obtained values of μ_i and f_r for the sample of ε_{pre} = 30% by fitting to the LLG equation. Within the experimental test of 2000 stretching cycles, μ_i can be tuned around 211, 142, and 87, whereas f_r is approximately at 3.19, 3.61, and 3.92 GHz for the applied tensile strains at 25, 15, and 0, respectively. The variation in μ_i is less than 9 and the variation in f_r is less than 0.17 GHz. Figure 6c, d, respectively, display μ_i and f_r for the film of ε_{pre} = 50% obtained at different stretching cycles. When the applied stretching strains are 45, 35, 25, and 0, μ_i remains around 158, 119, 90, and 50 within a variation less than 7, whereas f_r is maintained around 3.55, 3.79, 3.95, and 4.19 GHz within a variation less than 0.09 GHz. The nice repeatability for the strain tuning of high-frequency properties makes the wrinkled

https://doi.org/10.1021/acsami.1c07384
ACS Appl. Mater. Interfaces 2021, 13, 29975−29983

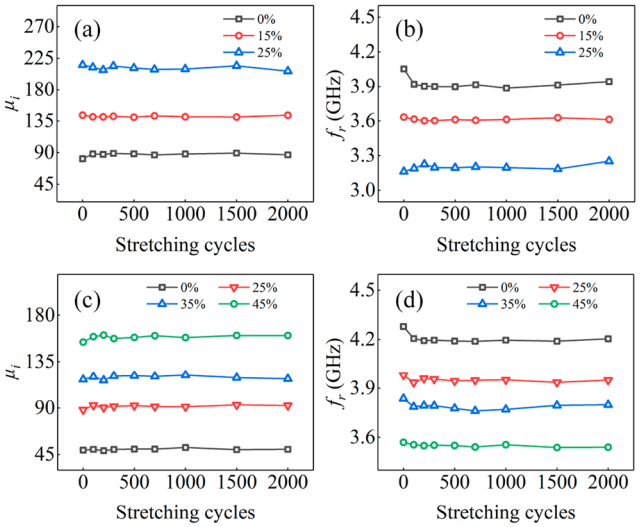

Figure 6. (a) Initial permeability and (b) ferromagnetic resonance frequency measured in the cyclic stretching test of 0 → 25% → 15% → 0 for the wrinkled CoFeB film fabricated with 30% prestrain. (c) Initial permeability and (d) ferromagnetic resonance frequency measured in the cyclic stretching test of 0 → 45% → 35% → 25% → 0 for the wrinkled CoFeB film fabricated with 50% prestrain. The permeability spectra are recorded at 0, 100, 200, 300, 500, 700, 1000, 1500, and 2000 stretching cycles, then fitted by the LLG equation to obtain the initial permeability and the ferromagnetic resonance frequency.

CoFeB films promising in the applications of tunable microwave devices.

CONCLUSION

In summary, we employed a self-assembled wrinkling surface structure on PDMS to fabricate flexible CoFeB films. They show a uniaxial magnetic anisotropy along the wrinkles and display good high-frequency performances with μ_i varied between 35 to 154 and f_r changed between 3.4 to 4.4 GHz by changing the prestrain. When a uniaxial tensile strain less than the prestrain is applied to the films, the wrinkling surface morphology is flattened and the residual tensile stress is relaxed. Thus, μ_i can be continuously varied in a range of hundreds and f_r can be changed in a range of 1 GHz. The results demonstrate a convenient method via applying uniaxial tensile strains to continuously tune the high-frequency properties of flexible magnetic thin films. The continuous tunability of the high-frequency performances of flexible magnetic films may open a new way to develop mechanical strain tunable flexible high-frequency devices, especially in wide-frequency-range applications.

METHODS

Sylgard-184 PDMS 30 vol % methylbenzene solution was spin-coated onto commercial PDMS membranes and dried in a vacuum oven at 95 °C for 12 h. The obtained PDMS membranes were 350 μm in thickness with a rms roughness of 3 nm. The PDMS membranes were stretched with different prestrains and mounted on a homemade stretching apparatus. Then, the CoFeB and Ta layers were sequentially sputtered onto the prestrained PDMS substrates in an ultrahigh vacuum magnetron sputtering system with a base pressure better than 6×10^{-7} Pa. Finally, the prestrain was released to obtain the wrinkling morphology of the CoFeB films. The surface morphologies were characterized by an optical microscope (Olympus MX51) and a scanning probe microscope (Bruker dimension icon). The hysteresis loops were measured by a vibrating sample magnetometer (Lakeshore 7404). The complex permeability spectra were recorded by a vector network analyzer (Keysight N5232B) with a shorted microstrip transmission-line perturbation method.

AUTHOR INFORMATION

Corresponding Authors

Guozhi Chai − *Key Laboratory for Magnetism and Magnetic Materials of the Ministry of Education, Lanzhou University, Lanzhou 730000, China*; Email: chaigzh@lzu.edu.cn

Qingfeng Zhan − *Key Laboratory of Polar Materials and Devices (MOE), School of Physics and Electronic Science, East China Normal University, Shanghai 200241, China*; Email: qfzhan@phy.ecnu.edu.cn

Authors

Jian Liu − *Key Laboratory of Polar Materials and Devices (MOE), School of Physics and Electronic Science, East China Normal University, Shanghai 200241, China*

Jinan Chen − *Key Laboratory of Polar Materials and Devices (MOE), School of Physics and Electronic Science, East China Normal University, Shanghai 200241, China*

Yanran Zhang − *Key Laboratory of Polar Materials and Devices (MOE), School of Physics and Electronic Science, East China Normal University, Shanghai 200241, China*

Shangjie Fu − *Key Laboratory of Polar Materials and Devices (MOE), School of Physics and Electronic Science, East China Normal University, Shanghai 200241, China*

Cuimei Cao − *Key Laboratory of Polar Materials and Devices (MOE), School of Physics and Electronic Science, East China Normal University, Shanghai 200241, China*

Xiaoyan Zhu − *Key Laboratory of Polar Materials and Devices (MOE), School of Physics and Electronic Science, East China Normal University, Shanghai 200241, China*

Yongbin Guo − *Engineering Research Center for Nanophotonics and Advanced Instrument, School of Physics and Electronic Science, East China Normal University, Shanghai 200241, China*

Wenjuan Cheng − *Key Laboratory of Polar Materials and Devices (MOE), School of Physics and Electronic Science, East China Normal University, Shanghai 200241, China*

Dongmei Jiang − *Key Laboratory of Polar Materials and Devices (MOE), School of Physics and Electronic Science, East China Normal University, Shanghai 200241, China*

Zhenjie Zhao − *Engineering Research Center for Nanophotonics and Advanced Instrument, School of Physics and Electronic Science, East China Normal University, Shanghai 200241, China*; orcid.org/0000-0001-5366-4896

Complete contact information is available at: https://pubs.acs.org/10.1021/acsami.1c07384

Notes

The authors declare no competing financial interest.

ACKNOWLEDGMENTS

This work was supported by the National Natural Science Foundation of China (11874150 and 11674336).

REFERENCES

(1) Osaka, T.; Takai, M.; Hayashi, K.; Ohashi, K.; Saito, M.; Yamada, K. A Soft Magnetic CoNiFe Film with High Saturation

Magnetic Flux Density and Low Coercivity. *Nature* **1998**, *392* (6678), 796−798.
(2) Chen, X.; Ma, Y. G.; Ong, C. K. Magnetic Anisotropy and Resonance Frequency of Patterned Soft Magnetic Strips. *J. Appl. Phys.* **2008**, *104* (1), 013921.
(3) Vas'ko, V. A.; Inturi, V. R.; Riemer, S. C.; Morrone, A.; Schouweiler, D.; Knox, R. D.; Kief, M. T. High Saturation Magnetization ilms of FeCoCr. *J. Appl. Phys.* **2002**, *91* (10), 6818−6820.
(4) Jin, S.; Zhu, W.; Tiefel, T. H.; Korenivski, V.; van Dover, R. B.; Chen, L. H. Fe-Cr-N Soft FMagnetic Thin Films. *J. Appl. Phys.* **1997**, *81* (8), 4042−4044.
(5) Han, X. M.; Ma, J. H.; Wang, Z.; Yao, Y. L.; Zuo, Y. L.; Xi, L.; Xue, D. S. Tunable In-plane Uniaxial Anisotropy and The Magnetization Reversal Mechanism of Patterned High-frequency Soft Magnetic FeTa strips. *J. Phys. D: Appl. Phys.* **2013**, *46* (48), 485004.
(6) Phuoc, N. N.; Ong, C. K. Observation of Magnetic Anisotropy Increment with Temperature in Composition-graded FeCoZr Thin Films. *Appl. Phys. Lett.* **2013**, *102* (21), 212406.
(7) Lou, Z.; Wang, L.; Shen, G. Recent Advances in Smart Wearable Sensing Systems. *Advanced Materials Technologies* **2018**, *3* (12), 1800444.
(8) Liu, C.; Cai, J.; Li, X.; Zhang, W.; Zhang, D. Flexible and Tunable Electromagnetic Meta-atom Based on Silver Nanowire Networks. *Mater. Des.* **2019**, *181*, 107982.
(9) Sun, L.; Qin, G.; Huang, H.; Zhou, H.; Behdad, N.; Zhou, W.; Ma, Z. Flexible High-frequency Microwave Inductors and Capacitors Integrated on a Polyethylene Terephthalate Substrate. *Appl. Phys. Lett.* **2010**, *96* (1), 013509.
(10) Yang, F. F.; Yan, S. S.; Yu, M. X.; Kang, S. S.; Dai, Y. Y.; Chen, Y. X.; Pan, S. B.; Zhang, J. L.; Bai, H. L.; Zhu, D. P.; Qiao, S. Z.; Pan, W. W.; Liu, G. L.; Mei, L. M. Soft Magnetic and High-frequency Properties of FeCoB−SiO2 Granular Films Deposited on Flexible Substrates. *J. Alloys Compd.* **2013**, *558*, 91−94.
(11) Tong, S.-Y.; Wu, J.-M.; Huang, Y.-T.; Tung, M.-J.; Ko, W.-S.; Wang, L.-C.; Yang, M.-D. Design and Characteristics of Flexible Radio-wave Absorber Consisted of Functional NiCuZn Ferrite−polymer Composites. *J. Alloys Compd.* **2011**, *509* (5), 2263−2268.
(12) Zuo, H.; Ge, S.; Wang, Z.; Xiao, Y.; Yao, D. Soft Magnetic Fe−Co−Si/native Oxide Multilayer Films on Flexible Substrates for High-frequency Applications. *Scr. Mater.* **2010**, *62* (10), 766−769.
(13) Jang, T.; Youn, H.; Shin, Y. J.; Guo, L. J. Transparent and Flexible Polarization-Independent Microwave Broadband Absorber. *ACS Photonics* **2014**, *1* (3), 279−284.
(14) Liu, W.; Shen, Y.; Xiao, G.; She, X.; Wang, J.; Jin, C. Mechanically Tunable Sub-10 nm Metal Gap by Stretching PDMS Substrate. *Nanotechnology* **2017**, *28* (7), 075301.
(15) Yang, S.; Liu, P.; Yang, M.; Wang, Q.; Song, J.; Dong, L. From Flexible and Stretchable Meta-Atom to Metamaterial: A Wearable Microwave Meta-Skin with Tunable Frequency Selective and Cloaking Effects. *Sci. Rep.* **2016**, *6* (1), 21921.
(16) Li, J.; Shah, C. M.; Withayachumnankul, W.; Ung, B. S. Y.; Mitchell, A.; Sriram, S.; Bhaskaran, M.; Chang, S.; Abbott, D. Mechanically Tunable Terahertz Metamaterials. *Appl. Phys. Lett.* **2013**, *102* (12), 121101.
(17) Gutruf, P.; Zou, C.; Withayachumnankul, W.; Bhaskaran, M.; Sriram, S.; Fumeaux, C. Mechanically Tunable Dielectric Resonator Metasurfaces at Visible Frequencies. *ACS Nano* **2016**, *10* (1), 133−141.
(18) Liu, Y.; Chen, L.; Tan, C. Y.; Liu, H. J.; Ong, C. K. Broadband Complex Permeability Characterization of Magnetic Thin Films using Shorted Microstrip Transmission-line Perturbation. *Rev. Sci. Instrum.* **2005**, *76* (6), 063911.
(19) Fan, X.; Xue, D.; Lin, M.; Zhang, Z.; Guo, D.; Jiang, C.; Wei, J. In Situ Fabrication of Co90Nb10 Soft Magnetic Thin Films with Adjustable Resonance Frequency from 1.3 to 4.9 GHz. *Appl. Phys. Lett.* **2008**, *92* (22), 222505.
(20) Yoo, J. H.; Restorff, J. B.; Wun-Fogle, M.; Flatau, A. B. The Effect of Magnetic Field Annealing on Single Crystal Iron Gallium Alloy. *J. Appl. Phys.* **2008**, *103* (7), 07B325.
(21) Kuanr, B. K.; Camley, R. E.; Celinski, Z. Exchange bias of NiO/NiFe: Linewidth Broadening and Anomalous Spin-wave Damping. *J. Appl. Phys.* **2003**, *93* (10), 7723−7725.
(22) Li, C.; Chai, G.; Yang, C.; Wang, W.; Xue, D. Tunable Zero-field Ferromagnetic Resonance Frequency from S to X Band in Oblique Deposited CoFeB Thin Films. *Sci. Rep.* **2015**, *5* (1), 17023.
(23) Li, S.; Xue, Q.; Du, H.; Xu, J.; Li, Q.; Shi, Z.; Gao, X.; Liu, M.; Nan, T.; Hu, Z.; Sun, N. X.; Shao, W. Large E-field Tunability of Magnetic Anisotropy and Ferromagnetic Resonance Frequency of Co-sputtered Fe50Co50-B Film. *J. Appl. Phys.* **2015**, *117* (17), 17D702.
(24) Lou, J.; Liu, M.; Reed, D.; Ren, Y.; Sun, N. X. Giant Electric Field Tuning of Magnetism in Novel Multiferroic FeGaB/Lead Zinc Niobate−Lead Titanate (PZN-PT) Heterostructures. *Adv. Mater.* **2009**, *21* (46), 4711−4715.
(25) Dai, G.; Zhan, Q.; Liu, Y.; Yang, H.; Zhang, X.; Chen, B.; Li, R.-W. Mechanically Tunable Magnetic Properties of Fe81Ga19 Films Grown on Flexible Substrates. *Appl. Phys. Lett.* **2012**, *100* (12), 122407.
(26) Yu, Y.; Zhan, Q.; Wei, J.; Wang, J.; Dai, G.; Zuo, Z.; Zhang, X.; Liu, Y.; Yang, H.; Zhang, Y.; Xie, S.; Wang, B.; Li, R.-W. Static and High Frequency Magnetic Properties of FeGa Thin Films Deposited on Convex Flexible Substrates. *Appl. Phys. Lett.* **2015**, *106* (16), 162405.
(27) Li, J.; Zhan, Q.; Zhang, S.; Wei, J.; Wang, J.; Pan, M.; Xie, Y.; Yang, H.; Zhou, Z.; Xie, S.; Wang, B.; Li, R.-W. Magnetic Anisotropy and High-frequency Property of Flexible FeCoTa Films Obliquely Deposited on a Wrinkled Topography. *Sci. Rep.* **2017**, *7* (1), 2837.
(28) Kim, D.-H.; Ahn, J.-H.; Choi, W. M.; Kim, H.-S.; Kim, T.-H.; Song, J.; Huang, Y. Y.; Liu, Z.; Lu, C.; Rogers, J. A. Stretchable and Foldable Silicon Integrated Circuits. *Science* **2008**, *320* (5875), 507−511.
(29) Jiang, H.; Khang, D.-Y.; Song, J.; Sun, Y.; Huang, Y.; Rogers, J. A. Finite Deformation Mechanics in Buckled Thin Films on Compliant Supports. *Proc. Natl. Acad. Sci. U. S. A.* **2007**, *104* (40), 15607−15612.
(30) Tang, Z.; Ni, H.; Lu, B.; Zheng, M.; Huang, Y.-A.; Lu, S.-G.; Tang, M.; Gao, J. Thickness Dependence of Magnetic Anisotropy and Domains in Amorphous Co40Fe40B20 Thin Films Grown on PET Flexible Substrates. *J. Magn. Magn. Mater.* **2017**, *426*, 444−449.
(31) Khang, D. Y.; Jiang, H.; Huang, Y.; Rogers, J. A. A Stretchable Form of Single-crystal Silicon for High-performance Electronics on Rubber Substrates. *Science* **2006**, *311* (5758), 208−212.
(32) Li, H.; Zhan, Q.; Liu, Y.; Liu, L.; Yang, H.; Zuo, Z.; Shang, T.; Wang, B.; Li, R.-W. Stretchable Spin Valve with Stable Magnetic Field Sensitivity by Ribbon-Patterned Periodic Wrinkles. *ACS Nano* **2016**, *10* (4), 4403−4409.
(33) Wang, D.; Nordman, C.; Qian, Z.; Daughton, J. M.; Myers, J. Magnetostriction Effect of Amorphous CoFeB Thin Films and Application in Spin-dependent Tunnel Junctions. *J. Appl. Phys.* **2005**, *97* (10), 10C906.
(34) Zhang, S.; Zhan, Q.; Yu, Y.; Liu, L.; Li, H.; Yang, H.; Xie, Y.; Wang, B.; Xie, S.; Li, R.-W. Surface Morphology and Magnetic Property of Wrinkled FeGa Thin Films Fabricated on Elastic Polydimethylsiloxane. *Appl. Phys. Lett.* **2016**, *108* (10), 102409.
(35) Grimsditch, M.; Jaccard, Y.; Schuller, I. K. Magnetic anisotropies in dot arrays: Shape anisotropy versus coupling. *Phys. Rev. B: Condens. Matter Mater. Phys.* **1998**, *58* (17), 11539−11543.
(36) Wei, J.; Wang, J.; Liu, Q.; Li, X.; Cao, D.; Sun, X. An Induction Method to Calculate the Complex Permeability of Soft Magnetic Films without a Reference Sample. *Rev. Sci. Instrum.* **2014**, *85* (5), 054705.
(37) McMichael, R. D.; Twisselmann, D. J.; Kunz, A. Localized Ferromagnetic Resonance in Inhomogeneous Thin Films. *Phys. Rev. Lett.* **2003**, *90* (22), 227601.

https://doi.org/10.1021/acsami.1c07384
ACS Appl. Mater. Interfaces 2021, 13, 29975−29983

(38) Phuoc, N. N.; Xu, F.; Ong, C. K. Ultrawideband Microwave Noise Filter: Hybrid Antiferromagnet/ferromagnet Exchange-coupled Multilayers. *Appl. Phys. Lett.* **2009**, *94* (9), 092505.
(39) Kittel; Charles. Interpretation of Anomalous Larmor Frequencies in Ferromagnetic Resonance Experiment. *Phys. Rev.* **1947**, *71* (4), 270−271.

https://doi.org/10.1021/acsami.1c07384
ACS Appl. Mater. Interfaces 2021, 13, 29975−29983